ICMIEE20-021

Evaluation of the Electrochemical Capacitor Performance of MnO_2-NiO Nanoparticles Prepared by the Simple Gel Formation Method

Yeasin A. Tarek[1], *Hridoy Roy*[2], *Ragib Shakil*[1], *Akter H. Reaz*[1], *Sanjida Afrin*[1], *Chanchal K. Roy*[1], *and Shakhawat H. Firoz*[1]*
[1] Department of Chemistry, Bangladesh University of Engineering and Technology, Dhaka-1000.
[2] Department of Chemical Engineering, Bangladesh University of Engineering and Technology, Dhaka-1000.

ABSTRACT
The unique features like fast charge-discharging, high power density, and extensive cycle life of energy materials are highly desirable for developing high-performance electrochemical supercapacitors. In this study, a binary transition metal oxide of manganese and nickel (MnO_2-NiO) was prepared via a facile gel formation method. A mixed metal oxide gel was prepared by the redox reaction between potassium permanganate and glycerol in the presence of pre-prepared nickel hydroxide. The MnO_2-NiO was obtained by heat-treatment at 650 °C temperature. The electrochemical capacitance performance was evaluated using cyclic voltammetry (CV) and galvanostatic charge-discharge (GCD) in a single compartment three-electrode system with 0.5 M Na_2SO_4 aqueous electrolyte solution. The heat-treated MnO_2-NiO demonstrated deviated pseudo capacitance behavior. The GCD has deviated from the symmetrical shape which allies with CV curves. However, the CV and GCD results indicated the fast-electrochemical response, good conductivity, and redox reversibility of the material. The MnO_2-NiO nanocomposite revealed a specific capacitance of 450 Fg^{-1} at 0.5 Ag^{-1} current density. Interestingly, this electrode material showed higher specific capacitance as compared to neat MnO_2, which is associated with the collaborative actions of mixed oxide as well as the porosity of material. Here the hybrid structure of the material offers a better solid electrolyte interface (SEI), and more active sites with more surface area for electrolyte charge intercalation and deintercalation. The binary oxide electrode material reported here exhibited an excellent choice for high-performance supercapacitor devices of large-scale applications.

Keywords: Supercapacitor, metal oxides, nanocomposites, binary mixed oxides.

1. Introduction

The development of clean, alternative, and novel energy storage systems has the ultimate desire of the present scientific community because of the rapid consumption of natural fuels and therefore the ascent of environmental contaminations [1]. The supercapacitors are a promising and impactful alternative to batteries for their unique advantages *viz*. fast charge/discharging, high power density, and large cycle life [2]. Two types of materials have been developed for electrochemical supercapacitor applications. Electrochemical double-layer supercapacitors (EDLC) where the charge is accumulated and released on electrode–electrode interfaces and in pseudo capacitors charge is transferred through the Faradic reaction between electrolyte and electrode [3, 4]. Carbonaceous materials are very suitable for EDLC. However, conducting polymers and transition metal oxides have gained attention for pseudo capacitors applications. In the pseudo capacitors, high specific capacitance is attained for the fast and reversible Faradic redox reactions [5]. For the development of high-performance pseudo capacitors applications, the transition metal oxides have great potential for their variable valency, diverse morphology, and suitable structures [5]. Ruthenium oxide (RuO_2) is one of the potential pseudo capacitance material which has already demonstrated high specific capacitance and stability [6]. However, the unavailability and cost are the great concerns for large-scale applications of the material. Other transition available metal oxides such as Co_3O_4 [8], CuO [1] and V_2O_5 [9] have also emerged, but they possess poor electrical conductivity. MnO_2 is an alternative and potent transition metal oxide which has shown its potential mostly due to its natural abundance, low cost, less toxicity and large theoretical specific capacity (~ 1370 Fg^{-1}) [5, 7]. However, morphology of the materials plays important role in the capacitance performance. In a recent study, it has been observed that the short diffusion depth makes the transfer of electron faster, but the electrons near the surface of electroactive manganese oxides are hindered for the participation in the electrochemical process as well as for the morphological differences [5]. That is why, synthesis of the nanoarchitectured nanomaterials of MnO_2 having appropriate morphologies as well as extremely porous nanostructure with high extent, and bigger pore volume was obtained by using different approaches. [10]. Here, incorporation of porous metal as substrates, conductive polymers, carbonaceous moiety like graphene, CNT etc. have been explored recently to enhance the specific capacitance of MnO_2 [11].

Nickel oxide (NiO) is of the most prominent pseudocapacitive materials studied so far which possesses a high theoretical capacitance (2573 Fg^{-1}) with an excellent electrochemical reactivity during the reaction process. NiO is also highly abundant in nature which facilitates the cost minimization, and due to its less toxic effect it is eco-friendly in nature [5].

* Corresponding author. Tel.: +88-01730713767
E-mail addresses: shfiroz@chem.buet.ac.bd

Designing a new material with the combination of multiple components and their specific properties is a new dimension to improve the electrochemical performances. Properly integrated individual components can provide synergistic effects which is basically responsible for the elevation of the specific capacitance [12]. The controlled growth of 3D hierarchical hetero-structures provide faster ions and electrons transport due to the improvement in the surface morphology. Factually, these improvements provide effective and faster intercalation-deintercalation of ions in the electrode materials. Thus, improved electrochemical performance can only be achieved in the intentionally designed nanoarchitectured nanomaterials which possess faster charging-discharging rates than a neat electrode material.

Throughout the literature the capacitive performances of NiO and MnO_2 have been widely discussed separately [13, 14]. In recent years, different research groups such as Liu et al. has reported a composite of NiO/MnO_2 in the stainless-steel substrate which has an areal capacitance (0.35 Fcm^{-2})[15]. Li et al. fabricated NiO/MnO_2 nanosheets by the hydrothermal method and found capacitance (1.0 Fcm^{-2}) [16]. NiO@MnO_2 core/shell nanocomposites fabricated by Junjiao Chen et al. through multiple steps that revealed a capacity of 266.7 Fg^{-1} at 0.5 Ag^{-1} [17]. Microwave-assisted synthesis of NiO/MnO_2 composite was performed by Bi et al. which showed 102.78 $mAhg^{-1}$ at 1 Ag^{-1} [18]. Moreover, free-standing nanostructures of NiO acts as a backbone or substrate to support primary electrode materials MnO_2 and results in hierarchical 3D hybrid or porous binary nanostructures. As it is well known that both the well-structured core and shell materials are excellent as pseudo capacitive materials, the composites of binary metal oxides can induce the synergistic effect of all individual constituents at a time and thus promotes the electrochemical performance of supercapacitor electrodes. The binary nanostructure materials are highly suggested as it facilitates more surface for ions adsorption and desorption on bulk active materials as electrodes. However, the synthetic procedures for these MnO_2-NiO binary structures are relatively complicated through a single route without using a template. To our best knowledge, there is no easier method to synthesized MnO_2-NiO nanocomposite till the date. In this paper, we have presented a simple gel formation method for synthesis of binary nanocomposite of MnO_2-NiO nanocomposite.

2. Experimental

2.1 Materials and reagents

Potassium permanganate ($KMnO_4$)(Merck, India), nickel chloride ($NiCl_2.6H_2O$)(Merck, India), glycerol (JHD, China), sodium hydroxide (NaOH) (Merck, India), sodium thiosulfate ($Na_2S_2O_3$) (Merck, Germany), polyvinylidene fluoride (Merck, Germany), dimethyl sulfoxide (DMSO) (Lab-Scan, Ireland) and ethanol (Merck, Germany) were purchased and used without further purification. A centrifuge machine (Universal 16A, Hettich, Germany) was used for separating the product from the solution. A hot air oven (DSO-500D, Digisystem, Taiwan) was used to dry materials. A high-temperature furnace ((LT 5/12, Nabertherm, Germany) was used for heating composite nanomaterials. Electrodes were fabricated using graphite rods with an exposed circular surface area of 0.28 cm^2. An ultrasonic bath was used for sonication purposes. Electrochemical experiments were carried out using a computer-controlled electrochemical workstation (CHI 660E, CHI Instruments, USA).

2.2 Preparation of MnO_2-NiO nanocomposite

A simple and economical one-step gel formation method was used for the synthesis of MnO_2-NiO nanocomposite. Briefly, 0.3 M potassium permanganate and 0.27 M $NiCl_2{\cdot}6H_2O$ were obtained separately through dissolving enough $KMnO_4$ and $NiCl_2{\cdot}6H_2O$ under continuous stirring for 30 min and subsequent ultra-sonication for 1 hour. 50 mL $NiCl_2{\cdot}6H_2O$ solution was mixed with 0.4 g NaOH. Then the basic solution of $NiCl_2{\cdot}6H_2O$ and 0.3 M glycerol were simultaneously added dropwise in $KMnO_4$ solution with the help of two separate burettes with vigorous magnetic stirring at room temperature. The resultant mixture allowed to settle down and kept undisturbed for 24 hours. A solid product was separated and washed with deionized water for several times. The product was centrifuged several times to ensure the removal of excess K^+ ion. The solid was then dried at 80 °C in a hot air electric oven and collected as black-brown powder. The dried black-brown powder was then heated at 650 °C for 6 hours in a muffle furnace under air atmosphere. For comparison with MnO_2-NiO nanocomposite, neat MnO_2 was prepared separately by following our previous work [26].

2.3 Electrochemical characterization

Electrochemical characterization of the prepared nanomaterials was evaluated using three-electrode systems through cyclic voltammetry (CV) and galvanostatic charge, and discharge (GCD). A single compartment cell with a modified graphite rod having an exposed surface of ~ 0.28 cm^2, used as the working electrode, as counter electrode platinum wire was used and Silver/Silver Chloride as a reference electrode. The modification of the graphite electrode was performed by improved solvent casting and drop drying method [19, 20]. In brief, the surface of the graphite electrode was cleaned by polishing mechanically and then dried at 50 °C in an oven under vacuum for 3 hours. A homogeneous slurry of active nanomaterials (15-20 mg) was prepared with 10 % PVDF as a binder for active material, 100 µL ethanol, and 250 µL DMSO which

were subjected to sonication in an ultrasonic bath for 30 min. A 5-10 µL of the homogeneous slurry was cast on a weighted graphite electrode surface dropwise with a micropipette. The casted graphite electrode was then dried at 50 °C in hot air oven for 4 hours. A thin film of the active materials was formed on the graphite surface. Finally, the modified graphite electrode was taken out from the oven, cooled in a desiccator and the constant weight was recorded. The amount of active material loaded on the electrode surface was about 1-2 mgcm^{-2}. All the experiments of CV and GCD were conducted with a freshly prepared 0.5 M Na_2SO_4 aqueous electrolyte solution to ensure sufficient conductivity. CV measurements were performed within a stable potential window (−0.4 to 0.3) V at different scan rates (5, 10, 20, 50, 100 mVs^{-1}). GCD experiments were performed at different current densities (0.1, 1, 2 Ag^{-1}) within a fixed potential range −0.4 to 0.3 V. For the three-electrode system, the specific capacitance (C_{sp}), energy density (E) and power density (P) were calculated from discharging time of GCD using the following equations [21],

$$C_{sp}\ (\mathrm{Fg^{-1}}) = \frac{I\Delta t}{m\Delta V} \qquad (1)$$

$$E\ (\mathrm{Whkg^{-1}}) = \frac{C_{sp}(\Delta V)^2 \times 1000}{2\times 3600} \qquad (2)$$

$$P\ (\mathrm{Wkg^{-1}}) = \frac{E\times 3600}{\Delta t} \qquad (3)$$

3. Results and discussions

Scheme of the synthesis procedure of neat MnO_2 and NiO as well as composite MnO_2-NiO is shown in Figure 1. It is desirable for the pseudo capacitor electrode materials to have high energy density along with high redox reversibility [22].

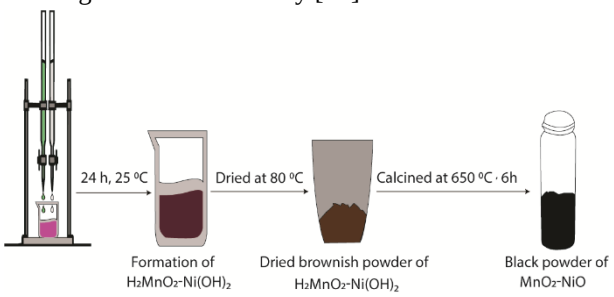

Figure-1. Scheme of the synthesis procedure of MnO_2-NiO nanomaterial.

The electrochemical performance of the prepared nanomaterials was studied through CV and GCD. The electrochemical measurements were performed in a single compartment three-electrode system using 0.5 M aqueous Na_2SO_4 electrolyte. The comparative CVs of MnO_2 (before annealing), MnO_2 (after annealing), MnO_2-NiO (before annealing), and MnO_2-NiO (after annealing) at scan rate 5 mVs^{-1} within the potential range of −0.4 to 0.3 V is shown in Figure 2. The wide positive and negative regions of CVs indicate that all nanomaterials have a good electrochemical response with good redox capacity, showing a fast and reversible

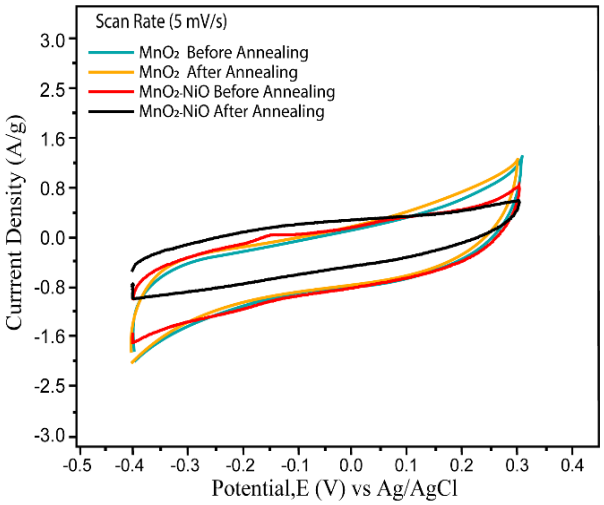

redox reaction taking place.

Figure 2. Comparative CV curves of prepared nanomaterials measured 0.5 M Na_2SO_4 (vs. Ag/AgCl).

All CV curves appear as rectangular shaped without obvious redox peaks except a small redox peak appeared for MnO_2-NiO (before annealing) which indicated good capacitive behavior. As CVs of MnO_2 (before annealing), MnO_2 (after annealing), MnO_2-NiO (before annealing) have a good rectangular shape compared to MnO_2-NiO (after annealing) which indicates the contribution of pseudo-capacitance in MnO_2-NiO (after annealing) is higher than others that attributed to the direct reversible redox reaction among Mn^{3+} and Mn^{4+} under applied potential range and the advantages of morphological changes after annealing at high temperature for super capacitive performance. Also, the introduction of NiO in the matrix of MnO_2 which stimulate the cation surface activty (Ni^{2+}) with the electrolyte as well as the insertion-desertion of Ni^{2+} through the porous structure of the MnO_2 matrix [23]. Interestingly, in MnO_2-NiO (after annealing), the pseudocapacitive characteristic of active materials is more prominent as compared to EDLC which suggested the distortion of CV shape perfect rectangular to distort parallelogram-like shapes. The distort parallelogram-like shapes correspond to the fast electrochemical response of the material and confirmed the satisfying high electrical conductivity due to redox pairs corresponding to reversible reactions of Ni^{+}/Ni^{2+} and Mn^{3+}/Mn^{4+} through the porous MnO_2 matrix in MnO_2-NiO (after annealing) [24]. It has been also observed that the rectangular shape CV of MnO_2 (before annealing), MnO_2 (after annealing), and MnO_2-NiO (before annealing) indicates having good charging rate capability due to EDLC without any contribution of pseudo capacitance. The CVs of MnO_2 (before annealing), MnO_2 (after annealing), MnO_2-NiO (before annealing), and MnO_2-NiO (after annealing) at various

scan rates indicated that even at high scan rates, good conductivity along with high electrochemical reversibility and stability are retained [25,27,28,29].

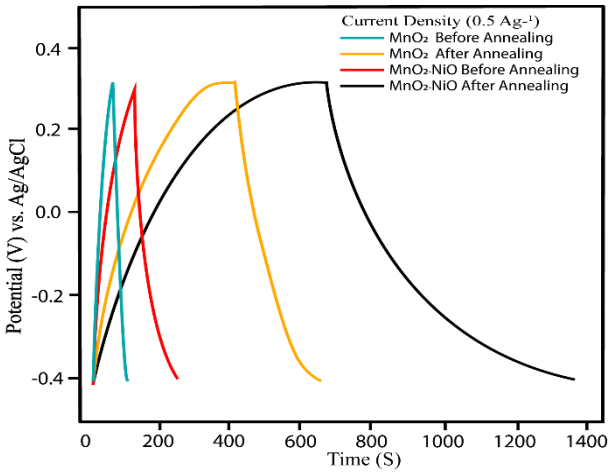

Figure 3. Comparative GCD curves of prepared nanomaterials in aqueous 0.5 M Na_2SO_4.

The anticipated characteristics of MnO_2 (before annealing), MnO_2 (after annealing), MnO_2-NiO (before annealing), and MnO_2-NiO (after annealing) were further analyzed through GCD at a current density of 0.5, 1.0 and 2.0 Ag^{-1} in 0.5 M aqueous Na_2SO_4

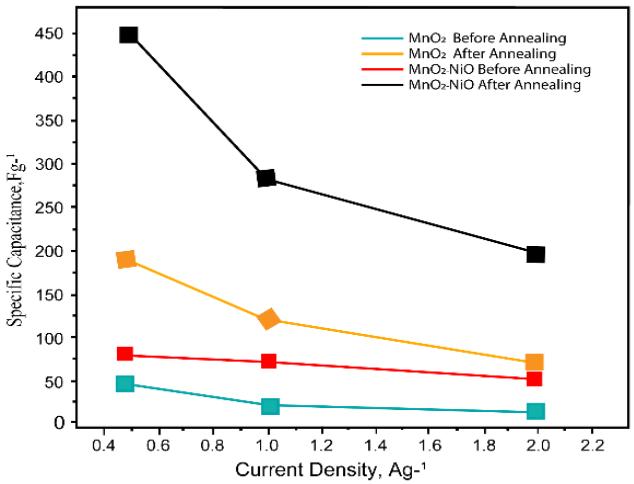

electrolyte within the

Figure 4. Comparative C_{sp} as a function of current densities of prepared nanomaterials.

stable potential ranges (−0.4 to 0.3) V. The comparative GCD profiles of MnO_2 (before annealing), MnO_2 (after annealing), MnO_2-NiO (before annealing), and MnO_2-NiO (after annealing) are shown in Figure 3**.** Slightly distorted symmetrical triangular nature of the GCD, indicated that the nature of the MnO_2-NiO (after annealing) composite material is pseudo capacitive type which is also supported by the obtained CV results. The higher discharging for MnO_2-NiO (after annealing) demonstrated that the electrolyte charge reservation is high and fast compared to MnO_2 (before annealing), MnO_2 (after annealing), MnO_2-NiO (before annealing) which may have attributed from the collaborative actions of manganese dioxide and nickel oxide merged into an shaped morphology. The effect of high current is analyzed by applying different current densities within the stable potential for MnO_2 (before annealing), MnO_2 (after annealing), MnO_2-NiO (before annealing), and MnO_2-NiO (after annealing). The GCD at different current densities demonstrated almost symmetrical triangle shape. The GCD at high current densities revealed that the introduction of different morphologies help in facile charge transfer capability. The C_{sp} of MnO_2 (before annealing), MnO_2 (after annealing), MnO_2-NiO (before annealing), and MnO_2-NiO (after annealing) were calculated using Equation-1 and presented in Figure-4.

The highest specific capacitance 450 Fg^{-1} was obtained from MnO_2-NiO electrodes at 0.5 Ag^{-1} among MnO_2 (before annealing) (50 Fg^{-1}), MnO_2 (after annealing) (192 Fg^{-1}) and MnO_2-NiO (before annealing) (78 Fg^{-1}). The result suggested that void space of MnO_2 integrated by NiO effectively improved the efficiency of electrode materials. The combined morphology MnO_2-NiO (after annealing) may be different from non-

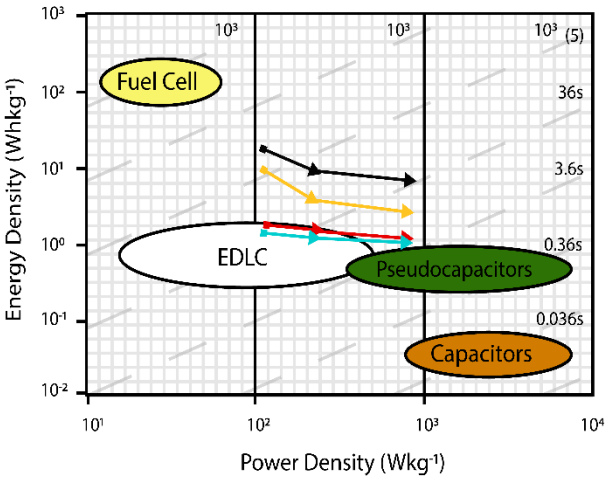

annealed MnO_2-NiO and pristine

Figure 5. Ragone plot of MnO_2 (before annealing), MnO2 (after annealing), MnO_2-NiO (before annealing) and MnO_2-NiO (after annealing).

MnO_2 which facilitated the mobility of the ions of electrolyte, as well as compensate volume switch to bypass the destruction of electrodes mophogy throughout the charging/discharg [34].

The MnO_2 of MnO_2-NiO (after annealing) may supply several paths as well as surfaces for storing ions. The insertion of ions into the void and porous electrode material having spacing and gaps between the internal and external MnO_2 layer may be created by the intercalation of NiO. Thus, the above merits are crucial for the superior super capacitive performance of MnO_2-

NiO (after annealing). Supercapacitor, which is usually represented by a diagram called the Ragone plot (Christen & Carlen2000). Two major parameters-energy density and power density are the crucial validation for the application of real-life. The energy density and power density were calculated using Equation-2 and Equation-3, respectively, and was depicted in Figure-5 as the Ragone plot of MnO_2 (before annealing), MnO_2 (after annealing), MnO_2-NiO (before annealing), and MnO_2-NiO (after annealing). Notably, the MnO_2-NiO (after annealing) electrode exhibits a maximum energy density (30.6 $Whkg^{-1}$) at a power density (175 Wkg^{-1}), which is much higher than that of MnO_2 (before annealing), MnO_2 (after annealing), MnO_2-NiO (before annealing). The above results anticipated that the present work is a good contribution to supercapacitor's materials as compared to the materials reported in Table 1.

Table 1: Electrochemical performances of the present NiO-MnO_2 composite

Composite Material	Method	Electrolyte	Specific Capacity (Fg^{-1})	Reference
MnO_2-based mixed oxides	Co-Precipitate	Na_2SO_4 (1.0 M)	210.0 Fg^{-1} (0.12 Ag^{-1})	[30]
Facile synthesis of Ni-Mn_2O_4	Hydrothermal	Na_2SO_4 (1.0 M)	370.5 Fg^{-1} (1.0 Ag^{-1})	[31]
MnO_2/graphene hydrogel	Hydrothermal	KOH (1.0 M)	278.5 Fg^{-1} (0.5 Ag^{-1})	[32]
Binary manganese–nickel oxides	Anodic deposition	Na_2SO_4 (0.1 M)	160.0 Fg^{-1} (1.0 Ag^{-1})	[33]
MnO_2-NiO binary oxide	Gel formation technique	Na_2SO_4 (0.5 M)	450.0 Fg^{-1} (0.5 Ag^{-1})	This work

4. Conclusion

The MnO_2-NiO were successfully prepared via a simple gel formation technique. This method provides facile and cost effective approach to prepare binary oxide of manganese and nickel oxide. Frequent transportation of electrolyte ions through the material is assisted by the structures of MnO_2-NiO. This the reason behind the improved active material loading on the working electrode. The MnO_2-NiO (after annealing) showed C_{sp} of 450 Fg^{-1} at 0.5 Ag^{-1} with an outstanding energy density and power density in 0.5 M Na_2SO_4 electrolyte. The hybrid morphology and the collaborative actions of MnO_2-NiO, the novel nanocomposite revealed a stable cycle performance and notable rate performance. We believe this work will pave the way of advancing proper metal-oxide based super capacitor material.

5. Acknowledgments

This work is funded by the Bangladesh University of Engineering and Technology (BUET), Dhaka, Bangladesh.

6. References

1) M.-J. Deng, C.-C. Wang, P.-J. Ho, C.-M. Lin, J.-M. Chen, and K.-T. Lu, *J. Mater. Chem. A*, vol. 2, no. 32, pp. 12857–12865, 2014.
2) X. Zhang *et al.*, *Sci. China Mater.*, vol. 62, no. 8, pp. 1115–1126, 2019.
3) F. Yao, D. T. Pham, and Y. H. Lee, *ChemSusChem*, vol. 8, no. 14, pp. 2284–2311, 2015.
4) K. M. Racik, K. Guruprasad, M. Mahendiran, J. Madhavan, T. Maiyalagan, and M. V. A. Raj, *J. Mater. Sci. Mater. Electron.*, vol. 30, no. 5, pp. 5222–5232, 2019.
5) S. Xi, Y. Zhu, Y. Yang, S. Jiang, and Z. Tang, *Nanoscale Res. Lett.*, vol. 12, no. 1, 2017.
6) L. Y. Chen, Y. Hou, J. L. Kang, A. Hirata, T. Fujita, and M. W. Chen, *Adv. Energy Mater.*, vol. 3, no. 7, pp. 851–856, 2013.
7) S. Goriparti, E. Miele, F. De Angelis, E. Di Fabrizio, R. Proietti Zaccaria, and C. Capiglia, *.J. Power Sources*, vol. 257, pp. 421–443, 2014.
8) Y. Li, B. Tan, and Y. Wu, *Nano Energy*, vol. 6, no. 1, pp. 265–270, 2008,
9) D. H. Nagaraju, Q. Wang, P. Beaujuge, and H. N. Alshareef, *J. Mater. Chem. A*, vol. 2, no. 40, pp. 17146–17152, 2014.
10) Zhu, S. J., Jia, J. Q., Wang, T., Zhao, D., Yang,

J., Dong, F., … Zhang, Y. X. (2015). *Communications*, *51*(80), 14840–14843.
11) M. Huang, F. Li, F. Dong, Y. X. Zhang, and L. L. Zhang, *J. Mater. Chem. A*, vol. 3, no. 43, pp. 21380–21423, 2015.
12) P. K. Panda, A. Grigoriev, Y. K. Mishra, and R. Ahuja, *Nanoscale Adv.*, vol. 2, no. 1, pp. 70–108, 2020.
13) B. Wang, J. S. Chen, Z. Wang, S. Madhavi, and X. W. Lou, *Adv. Energy Mater.*, vol. 2, no. 10, pp. 1188–1192, 2012.
14) Zhai, T., Xie, S., Yu, M., Fang, P., Liang, C., Lu, X., & Tong, Y. (2014). *Nano Energy*, *8*, 255–263.
15) Liu, D., Wang, Q., Qiao, L., Li, F., Wang, D., Yang, Z., & He, D. (2012). *Journal of Materials Chemistry*, *22*(2), 483–487.
16) L. Yang *et al.*, *Chem. - An Asian J.*, vol. 9, no. 6, pp. 1579–1585, 2014.
17) J. Chen, Y. Huang, C. Li, X. Chen, and X. Zhang, *Appl. Surf. Sci.*, vol. 360, pp. 534–539, 2016.
18) Y. Bi, A. Nautiyal, H. Zhang, J. Luo, and X. Zhang, *Electrochim. Acta*, vol. 260, pp. 952–958, 2018.
19) B. Moradi and G. G. Botte, *J. Appl. Electrochem.*, vol. 46, no. 2, pp. 123–148, 2016.
20) H. Wang, H. Yi, X. Chen, and X. Wang, *J. Mater. Chem. A*, vol. 2, no. 9, pp. 3223–3230, 2014.
21) Z. Wu, L. Li, J. M. Yan, and X. B. Zhang, *Adv. Sci.*, vol. 4, no. 6, 2017.
22) L. Bao, J. Zang, and X. Li, *Nano Lett.*, vol. 11, no. 3, pp. 1215–1220, 2011.
23) J. H. Kim, K. Zhu, Y. Yan, C. L. Perkins, and A. J. Frank, *Nano Lett.*, vol. 10, no. 10, pp. 4099–4104, 2010.
24) U. J. Chavan and A. A. Yadav, *J. Mater. Sci. Mater. Electron.*, vol. 28, no. 6, pp. 4958–4964, 2017.
25) L. Athouël, F. Moser, R. Dugas, O. Crosnier, D. Bélanger, and T. Brousse, *J. Phys. Chem. C*, vol. 112, no. 18, pp. 7270–7277, 2008.
26) Ullah, A. K. M. A., Kibria, A. K. M. F., Akter, M., Khan, M. N. I., Maksud, M. A., Jahan, R. A., & Firoz, S. H. *Journal of Saudi Chemical Society*, *21*(7), 830–836, 2017.
27) H. Kim and B. N. Popov, *J. Electrochem. Soc.*, vol. 150, no. 3, p. D56, 2003.
28) Zhong, J., Yi, F., Gao, A., Shu, D., Huang, Y., Li, Z., Zhao, S. (2017). *ChemElectroChem*, *4*(5), 1088–1094.
29) Y. S. Chen and C. C. Hu, *Electrochem. Solid-State Lett.*, vol. 6, no. 10, pp. 210–213, 2003.
30) Kim, H., and Popov, B. N, *Journal of The Electrochem. Soc*, *150*(3), D56.,2003.
31) Wei, H., Wang, J., Yu, L., Zhang, Y., Hou, D., &Li, T. *Ceramics International*, *42*(13), 14963–14969,2016.
32) Zhong, J., Yi, F., Gao, A., Shu, D., Huang, Y., Li,Z. Zhao, S, *Chem. Electrochem*, *4*(5), 1088–1094,2017.
33) Chen, Y. S., & Hu, C. C. *Electrochem. SolidStateLett*, *6*(10),2003.
34) Athouël, L., Moser, F., Dugas, R., Crosnier, O.,Bélanger, D., & Brousse, T. (2019). *ECS Transactions*, *16*(1), 119–123.

NOMENCLATURE

i/m : Current density, Ag^{-1}
Δt: Discharge time, s
E: Energy density, $Wh\ kg^{-1}$
C_{sp}: Specific capacitance, Fg^{-1}
ΔV: Potential window of discharge, V
P: Power density, Wkg^{-1}
I : Loaded current, A
m: Active mass, g